Bremsstrahlung from an Equilibrating Quark-Gluon Plasma *

Munshi G. Mustafa[1†] and Markus H. Thoma[2‡]
[1] *Institut für Theoretische Physik, Universität Giessen, 35392 Giessen, Germany*
[2] *Theory Division, CERN, CH-1211 Geneva 23, Switzerland*
(February 5, 2000)

Abstract

The photon production rate from a chemically equilibrating quark-gluon plasma likely to be produced at RHIC (BNL) and LHC (CERN) energies is computed taking into account bremsstrahlung. The plasma is assumed to be in local thermal equilibrium, but with a phase space distribution that deviates from the Fermi or Bose distribution by space-time dependent factors (fugacities). The photon spectrum is obtained by integrating the photon rate over the space-time history of the plasma, adopting a boost invariant cylindrically symmetric transverse expansion of the system with different nuclear profile functions. Initial conditions obtained from a self-screened parton cascade calculation and, for comparison, from the HIJING model are used. Compared to the equilibrium case a suppression of the photon yield by one to three orders of magnitude is observed. Furthermore the photon production due to bremsstrahlung from the chemically nonequilibrated plasma dominates over the emission from Compton scattering and quark-antiquark annihilation at LHC energies, whereas the both processes are of the same order at RHIC energies.

PACS numbers: 12.38.Mh, 24.10.Nz, 25.75.-q

*Supported by BMBF, GSI Darmstadt, DFG, and Humboldt foundation

†Humboldt fellow and on leave of absence from Saha Institute of Nuclear Physics, 1/AF Bidhan Nagar, Calcutta 700 064, India

‡Heisenberg fellow

I. INTRODUCTION

During the last two decades a substantial amount of activity, both experimentally and theoretically, has been devoted to an profound understanding of the so called quark-gluon plasma (QGP). This new state of matter is predicted to exist at high temperatures and/or high baryon densities, when a phase transition takes place from a hadronic to a quasi-free state of quarks and gluons [1–3]. Numerical solutions of QCD using lattice techniques suggest that the critical temperature (at zero baryon density) is about 160 MeV [4]. The relativistic heavy-ion collisions experiments (SPS, RHIC, LHC) are being studied with the intention of creating a QGP in the laboratory [1–3,5]. It is believed that the deconfined phase of quarks and gluons in or close to thermal equilibrium might be present in the hot and dense fireball of such nucleus-nucleus collisions for about 10 fm/c. Once produced, this plasma expands and becomes cooler and more dilute. If QCD admits a first-order deconfinement or chiral phase transition, the plasma will pass through a mixed phase of quarks, gluons, and hadrons, before the hadrons lose thermal contact and stream freely towards the detectors. The prime goal is to find a reliable signature which could confirm that a QGP has indeed been formed during the collision [6]. A tremendous amount of theoretical effort is underway to look for observable signatures for this new state of matter. Hadrons arriving in the detectors carry mainly information about the hadronic phase following the QGP in the expansion of the fireball. Among the proposed various signatures of the QGP, dileptons and photons have long been considered as a very promising and advantageous signal for the QGP formation [7–31]. Since these are electromagnetically interacting particles, once produced, they will escape from the medium without further interaction [32]. This makes them a unique probe as they carry information about the primordial state of the matter in heavy ion collisions.

Photons are produced at every stage of the collision, and in an expanding system their number is obtained by an integration over the four volume of the reaction zone. The emission of photons in heavy-ion collisions can be termed as direct and decay ones. The direct photons are emitted as a result of rescattering of charged particles in the hot matter. The decay photons, on the other hand, originate from the decay of final state hadrons, mainly from π^0 and η mesons, and can be estimated from an invariant mass analysis. In addition, one can also classify direct photons into prompt and thermal. Prompt photons are produced at the pre-equilibrium stage of an ultra-relativistic heavy ion reaction due to hard scattering processes among the partons of the initial colliding nuclei, which drive the system towards local thermal equilibrium. The contribution from the hard QCD processes is well understood within perturbative QCD. The thermal photons are emitted from the later stage when the fireball has reached local thermodynamic equilibrium. Once the thermal equilibration is achieved we have a copious production of large transverse momentum photons since the temperature is rather high. The transverse flow of the system is moderate at early time, and the production of high-p_T photons will only be marginally affected by flow. By the time flow and other aspect of the QGP develop, the temperature will be dropped considerably causing a production of low momentum photons. In addition, there will also be a substantial contribution from hadronic reactions. In order to make reliable predictions for the photon yield, we have to consider the photon production from all stages of the fireball. In this work, however, we will focus only on the emission of thermal photons from the QGP. In particular, we take into account the fact that the QGP may not be in chemical equilibrium, *i.e.*, the

phase space of the quarks and gluons may be undersaturated [29,33–37].

Almost a decade ago the production rate of photons from the QGP has been evaluated [15–17] at the one-loop level (Fig.1a) within the Hard Thermal Loop (HTL) resummation technique [38]. The production rate is related to the imaginary part of the polarisation diagram [39] corresponding to Compton scattering (Fig.1b) and quark-antiquark annihilation (Fig.1c). The rate, comprising the above two processes, has extensively been used in studying the photon spectrum [20–23,25–29,31] from the QGP. In addition, an interim attempt has been undertaken in studying the photons from the QGP due to bremsstrahlung processes [40–42] within the soft photon approximation [43,44]. At low transverse momentum this was found to contribute substantially to the production rate both in equilibrium [40,41] and in equilibrating [42] scenarios.

Recently Aurenche et al. [18,19] have also calculated bremsstrahlung of photons (real and virtual), at the two-loop level (Fig.2a), within the frame work of the effective perturbative expansion based on the HTL resummation technique. If the exchanged gluon in the two-loop diagrams is time-like, this corresponds to processes, which are in the case of hard real photons identical to Compton scattering and annihilation already discussed above [45]. Bremsstrahlung appears only on the two-loop level when the exchanged gluon in the two-loop polarisation diagram is space-like. Surprisingly the contributions of the physical processes arising from the two-loop diagram are of the same order in the coupling constant as those of the one-loop diagram. This is caused by an higher infrared sensitivity of the two-loop rate (bremsstrahlung), containing the exchange of a gluon and a collinear singularity for the photon emission, in contrast to the one-loop contributions (Compton scattering, annihilation), containing the exchange of a quark.

The photon production at the two-loop level represents two physical processes, namely the usual bremsstrahlung processes, given in Fig.2b, and a completely new mechanism (Fig.2c) describing the annihilation of a quark and an antiquark, where one of the particles is a product of the scattering with either a quark, a antiquark or a gluon. The photon production rate following from these processes dominates over the one-loop contribution, in particular for energetic photons as the contribution to the rate from the annihilation with scattering process is proportional to the photon energy.

Recently employing this new rates along with the one-loop contributions from the quark matter, the production of single photons has been reinvestigated [23,24] for an equilibrated plasma, taking into account the photon production also from the mixed and the hadronic phase. It has been found that the production rate is consistent with the measured upper limit in S + Au collisions at CERN SPS [46] by the WA80 experiment, and support a description where a QGP is formed. However, it has also been stated in Ref. [23] that a chemically non-equilibrated plasma can lead to a reduction of the photon yield from the quark phase, as the plasma likely to be produced in ultra-relativistic heavy ion collisions will probably be far away from the chemical equilibrium, showing a strong undersaturation of the phase space.

In the self-screened parton cascade (SSPC) model [47] early hard scatterings among partons produce a medium which screens the long range color fields associated with softer interactions. When two heavy nuclei collide at sufficiently high energy, the screening occurs on the length scale where perturbative QCD still applies. This approach yields predictions for the initial conditions of the forming QGP without the need of any ad-hoc virtuality

and momentum cut-off parameters. These calculations also show that the QGP likely to be formed at RHIC and LHC energies could be hot and initially far away from chemical equilibrium. With the passage of time, chemical reactions among the partons will push the system towards chemical equilibration initially, but the large transverse velocity gradient drives the system away from chemical equilibration at later stages [29,35,36]. It is quite evident that signals which are emitted from the QGP phase will be influenced and, on the other hand, also reflect the chemical evolution of the plasma. Therefore it will be interesting to study the production of single photons from the QGP using the two-loop results of Aurenche et al. [19] accompanied with the one-loop contributions in a chemically equilibrating plasma.

The paper is organized in the following way. In Sec.II, we briefly review the hydrodynamic and chemical evolution of the plasma through the partonic reactions taking a transverse expansion into account. We also discuss implications of different initial conditions and nuclear profile functions. In Sec.III, we present the photon production rates for an equilibrated and chemically non-equilibrated plasma. We also discuss the space-time evolution dynamics for obtaining the photon spectrum. The results of this calculation are presented in Sec.IV and finally, we give a brief summary in Sec.V.

II. HYDRODYNAMIC EXPANSION AND CHEMICAL EQUILIBRATION

We assume that kinetic equilibrium has been achieved when the momenta of the partons become locally isotropic. At collider energies it has been estimated that this happens at $\tau_i \approx 0.2 - 0.3$ fm/c [48]. Beyond this point the further expansion is described by hydrodynamic equations and the chemical equilibration is governed by a set of master equations which are driven by the two-body reactions ($gg \leftrightarrow q\bar{q}$) and gluon multiplication and its inverse process, gluon fusion ($gg \leftrightarrow ggg$). The elastic scattering processes help to maintain the thermal equilibrium. The hot matter continues to expand and cools due to expansion and chemical equilibration. We shall, somewhat arbitrarily, terminate the evolution once the energy density reaches some critical value (here taken as $\epsilon_f = 1.45$ GeV/fm^3 [49]).

The expansion of the system is described by the equation for conservation of energy and momentum of an ideal fluid:

$$\partial_\mu T^{\mu\nu} = 0 \,, \qquad T^{\mu\nu} = (\epsilon + P) u^\mu u^\nu + P g^{\mu\nu} \,, \tag{1}$$

where ϵ is the energy density and P is the pressure measured in the frame comoving with the fluid. The four-velocity vector u^μ of the fluid satisfies the constraint $u^2 = -1$. For a chemically equilibrating plasma the distribution functions for gluons and quarks are assumed to be proportional to the equilibrium distributions,

$$n_i(E, \lambda_i) = \lambda_i \tilde{n}_i(E) \quad , \tag{2}$$

where $\tilde{n}_i(E) = (e^{\beta E} \mp 1)^{-1}$ is the Bose (Fermi) distribution for gluons (quarks), and λ_i is the fugacity for the parton species i, which describes the deviation from chemical equilibrium. The fugacity factor takes into account the undersaturation of the parton phase space density, *i.e.*, $0 \leq \lambda_i \leq 1$. The equation of state for a partially equilibrated plasma of massless particles can be written as [33]

$$\epsilon = 3P = \left[a_2\lambda_g + b_2\left(\lambda_q + \lambda_{\bar{q}}\right)\right] T^4\,, \tag{3}$$

where $a_2 = 8\pi^2/15$, $b_2 = 7\pi^2 N_f/40$, and $N_f = 2.5$ is the number of dynamical quark flavors. Now, the density of an equilibrating partonic system can be written as

$$n_g = \lambda_g \tilde{n}_g, \qquad n_q = \lambda_q \tilde{n}_q, \tag{4}$$

where $\tilde{n}_i$ is the equilibrium density for the parton species i:

$$\tilde{n}_g = \frac{16}{\pi^2}\zeta(3)T^3 = a_1 T^3, \tag{5}$$

$$\tilde{n}_q = \frac{9}{2\pi^2}\zeta(3)N_f T^3 = b_1 T^3. \tag{6}$$

We further assume that $\lambda_q = \lambda_{\bar{q}}$, which holds at zero baryon density approximately valid at RHIC and LHC. The equation of state (3) implies the speed of sound $c_s = 1/\sqrt{3}$. We solve the hydrodynamic equations (1) with the assumption that the system undergoes a boost invariant longitudinal expansion along the z-axis and a cylindrically symmetric transverse expansion [50]. It is then sufficient to solve the problem for $z = 0$, because of the assumption of boost invariance.

The chemical equilibration of the species i is governed by the master equation

$$\partial_\mu\left(n_i u^\mu\right) = R_i(x) \quad , \tag{7}$$

where R_i are the rates which make the system proceed towards chemical equilibrium. The system would be in chemical equilibrium if $R_i(x) = 0$. The dominant chemical reactions through which the chemical equilibration proceeds [33] are $gg \leftrightarrow ggg$ and $gg \leftrightarrow q\bar{q}$. The above master rate equations for different species can be written as [33]

$$\begin{aligned}
\partial_\mu(n_g u^\mu) &= n_g(R_{2\to3} - R_{3\to2}) - \left(n_g R_{g\to q} - n_q R_{q\to g}\right), \\
\partial_\mu(n_q u^\mu) &= \partial_\mu(n_{\bar{q}} u^\mu) = n_g R_{g\to q} - n_q R_{q\to g},
\end{aligned} \tag{8}$$

in an obvious notation. The rates corresponding to those chemical reactions depend on the temperature and fugacities in a rather complicated way. However, following Ref. [33] the right hand side of the Eq.(8) can be simplified using the factorised distributions in Eq.(2), and the rate equations become

$$\begin{aligned}
\partial_t(n_g\gamma) + \partial_r\left(n_g\gamma v_r\right) + n_g\gamma\left(\frac{v_r}{r} + \frac{1}{t}\right) &= R_3 n_g\left(1 - \frac{n_g}{\tilde{n}_g}\right) - 2R_2 n_g\left(1 - \frac{n_q n_{\bar{q}}\tilde{n}_g^2}{\tilde{n}_q\tilde{n}_{\bar{q}}{n_g}^2}\right), \\
\partial_t(n_q\gamma) + \partial_r\left(n_q\gamma v_r\right) + n_q\gamma\left(\frac{v_r}{r} + \frac{1}{t}\right) &= R_2 n_g\left(1 - \frac{n_q n_{\bar{q}}\tilde{n}_g^2}{\tilde{n}_q\tilde{n}_{\bar{q}}{n_g}^2}\right),
\end{aligned} \tag{9}$$

where v_r is the transverse velocity and $\gamma = 1/\sqrt{1 - v_r^2}$. It is to be noted that the chemical evolution equation for antiquarks is same ($n_q = n_{\bar{q}}$) according to the assumption of a vanishing baryon density at RHIC and LHC. R_2 and R_3 are the density weighted rates of the chemical reactions, given by [33],

$$R_2 \approx 0.24 N_f \alpha_s^2 \lambda_g T \ln(1.65/\alpha_s \lambda_g),$$
$$R_3 = 2.1 \alpha_s^2 T (2\lambda_g - \lambda_g^2)^{1/2}, \tag{10}$$

where color Debye screening, effective temperature dependent quark masses, and the Landau - Pomeranchuk - Migdal effect, suppressing the induced gluon radiation, have been taken into account.

In order to solve the hydrodynamic and chemical master equations, one needs to specify the initial conditions. The initial conditions are tabulated in Table-I obtained from SSPC [47] and HIJING [51] models. The initial conditions denoted by (I) are the original HIJING predictions, while the set (II) is obtained by multiplying the original initial fugacities by a factor of 4 and by decreasing the initial temperature somewhat, in order to take into account possible uncertainties in the models such as the neglect of soft parton production from the color field [29]. The hydrodynamic equations (1) are solved numerically, with the initial conditions given in Table-I to get $\epsilon(r,t)$ and $v_r(r,t)$, which serve as input for the equations (9) describing the evolution of the fugacities of quarks and gluons.

In addition to the different initial conditions, we also need a nuclear profile function for the fireball to solve those equations numerically as the matter distribution with sharp edges are difficult to use in numerical simulations [50]. With appropriate nuclear profile functions one can smooth out the matter distribution at the surface of the initial fireball. In view of this it would be interesting and as well useful to explore the dependence of the evolution of the plasma on the various nuclear profile functions. For this purpose we consider in the following two nuclear profile functions. The first one is a Fermi-like profile function [50]

$$T_A(r) = \frac{1}{e^{(r-R_T)/\delta}+1} \quad , \tag{11}$$

where r is the transverse coordinate, R_T is the transverse radius of the nucleus and δ is the surface thickness. The evolution of $\epsilon(r,t)$, $v_r(r,t)$ and $\lambda_g(r,t)$ and $\lambda_q(r,t)$ with the Fermi profile function and different initial conditions are discussed in great detail in Refs. [29,35].

The second one is the wounded-nucleon profile [36] given as

$$T_A(r) = \frac{3}{2}\sqrt{1-\frac{r^2}{R_T^2}} \quad . \tag{12}$$

Since the initial conditions tabulated in Table-I describe averages over the transverse cross section, πR_T^2, of the colliding nuclei in a central collision, one needs to modify them for various nuclear profiles. This implies that the system will have higher initial energy density and fugacities using the wounded-nucleon profiles, but also the preexistence of a density gradient over the whole transverse area resulting in a faster onset of the transverse expansion throughout the plasma volume [36]. In Figs.3 and 4 we discuss briefly the evolution of the different parton fugacities with SSPC initial conditions and the wounded-nucleon profile for a transversely expanding plasma at RHIC and LHC energies. The evolution of $\epsilon(r,t)$ and $v_r(r,t)$ are given in Ref. [36] and we do not repeat them here. In the figures N denotes the time [52].

One observes that the quark fugacities (Fig.3) always lag behind the gluon fugacities (Fig.4). This is obvious as the SSPC model predicts a gluon dominated plasma. At both energies, the fugacities initially increase with time, then start decreasing because by then

the transverse expansion has set in (v_r is non-zero). Thus in regions where the transverse velocity is large (later times), the plasma moves farther away from chemical equilibrium. The reason is that the velocity gradient causes a depletion in the parton number in the fluid element, which could not be made up by the number of partons produced due to the chemical parton reactions [35], resulting in a decrease of the parton fugacities. The chemical equilibration cannot be achieved at RHIC as the life time of the plasma (4-5 fm/c) is too small. Due to the longer life time of the plasma phase at LHC energies ($\sim$ 10 fm/c), the effects of the transverse expansion are more dramatic, and the entire matter participates in the flow. There is a possibility of approaching chemical equilibration at LHC energies, but as soon as the velocity gradient becomes substantial ($N \geq 31$ corresponding to $\tau \simeq 6$ fm/c), the expansion begins to impede the chemical equilibration. As we shall see, this undersaturation of the parton phase space will have significant consequences in the photon production from the quark phase of the plasma. In the following section we obtain the photon production both from an equilibrated as well as an equilibrating plasma.

III. PHOTON PRODUCTION FROM QUARK-GLUON PLASMA

The thermal photon production can be evaluated in finite temperature QCD. The lowest order photon emitting processes in the QGP are Compton scattering and quark-antiquark annihilation given in Fig.1b and 1c, respectively, which follow from the one-loop photon polarisation diagram (Fig.1a) by applying the thermal cutting rules [53]. For massless fermions the corresponding rate encounters a logarithmic infrared singularity. Since the divergence is only logarithmic, it can consistently be cured by taking into account medium effects within the HTL resummation technique of the Braaten-Pisarski method [38], yielding the production rate of hard photons ($E >> T$) in thermal and chemical equilibrium [15,16]

$$E\,\frac{\mathrm{d}N_\gamma}{\mathrm{d}^4x\mathrm{d}^3p}\bigg|^{\mathsf{eq.}}_{\mathsf{com.+ann.}} = \frac{N_cC_F}{8\pi^2}\left(\sum_f e_f^2\right)\alpha\alpha_s\ln\left(\frac{cE}{\alpha_sT}\right)T^2e^{-E/T}, \tag{13}$$

where $c = 0.23$ is a constant, N_c is the number of colors, $C_F = 4/3$, e_f is the electric charge of the quark with flavor f in units of the electron charge e, and the sum runs over the number of quark flavors involved [54].

In order to estimate the effect of the chemical nonequilibrium, we follow the procedure described below and already used in Refs. [27,28,35]. This procedure has been shown to give reasonable results in the case of the one-loop contribution, if its results are compared to more elaborate approaches based on the HTL method generalized to nonequilibrium [20,55]. Here we adopt this simplified approach since HTL calculations of the photon production rate due to bremsstrahlung are very involved.

Considering the hard part of the photon rate one can assign fugacities to the external partons and also replace the infrared cut-off, which has to be introduced for regularizing a logarithmic infrared divergence using bare, massless quark propagators in the matrix elements, by twice the thermal quark mass. We also consider fugacities only in the entrance channel as the average momentum of the light partons is $\sim 3T$ rendering Pauli blocking and Bose enhancement effects negligible for our purpose. Taking into account the nonequilibrium effects in this way, the corresponding rate for the Compton process becomes

$$E\frac{\mathrm{d}N_\gamma}{\mathrm{d}^4x\,\mathrm{d}^3p}\bigg|_{\mathsf{com.}}^{\mathsf{ceq.}} = \frac{2\alpha\alpha_s}{\pi^4}\lambda_q\lambda_g T^2\left(\sum_f e_f^2\right)e^{-E/T}\left[\ln\left(\frac{4ET}{\kappa_c^2}\right)+\frac{1}{2}-C\right], \tag{14}$$

and the rate of the radiative annihilation process is given by

$$E\,\frac{\mathrm{d}N_\gamma}{\mathrm{d}^4x\,\mathrm{d}^3p}\bigg|_{\mathsf{ann.}}^{\mathsf{ceq.}} = \frac{2\alpha\alpha_s}{\pi^4}\lambda_q\lambda_{\bar{q}} T^2\left(\sum_f e_f^2\right)e^{-E/T}\left[\ln\left(\frac{4ET}{\kappa_c^2}\right)-1-C\right]. \tag{15}$$

Here $C = 0.577216\ldots$, and $\kappa_c = 2m_q^2$, where the thermal mass of the quarks in the non-equilibrated medium [27] is given as

$$m_q^2 = \frac{4\pi\alpha_s}{9}\left(\lambda_g+\frac{\lambda_q}{2}\right)T^2. \tag{16}$$

In the derivation of (14) and (15), the Boltzmann distribution has also been used for the final state parton (in accordance with neglecting Pauli blocking and Bose enhancement), whereas in (13) this approximation has been assumed only for the initial state partons [15]. Therefore, the sum of (14) and (15) does not agree with (13) in the equilibrium limit ($\lambda_g = \lambda_q = 1$). This minor correction, however, is unimportant for our purpose of estimating the non-equilibrium effect on the photon spectra.

As discussed the photon production due to bremsstrahlung only appears at the two-loop level, if the exchanged gluon is space like. The corresponding two-loop diagrams are given in Fig.2a. Cutting these diagram according to thermal cutting rules [53] leads to two important physical processes [19], which contribute at the same order in the coupling constant as the one-loop result given in eq.(13). One is the usual bremsstrahlung from quarks and antiquarks given in Fig.2b. The other one describes the quark-antiquark annihilation with scattering (abbreviated as aws) in the heat bath shown in Fig.2c. In the framework of the HTL technique, Aurenche et al. [19] obtained the corresponding equilibrium rates for the bremsstrahlung process as

$$E\,\frac{\mathrm{d}N_\gamma}{\mathrm{d}^4x\,\mathrm{d}^3p}\bigg|_{\mathsf{brem.}}^{\mathsf{eq.}} = \frac{2N_cC_F}{\pi^5}\alpha\alpha_s\left(\sum_f e_f^2\right)T^2e^{-E/T}(J_T-J_L)\ln(2)\ , \tag{17}$$

and for the annihilation with scattering process as

$$E\,\frac{\mathrm{d}N_\gamma}{\mathrm{d}^4x\,\mathrm{d}^3p}\bigg|_{\mathsf{aws}}^{\mathsf{eq.}} = \frac{2N_cC_F}{3\pi^5}\alpha\alpha_s\left(\sum_f e_f^2\right)ETe^{-E/T}(J_T-J_L)\ \ , \tag{18}$$

where for two flavors $J_T \approx 4.45$ and $J_L \approx -4.26$.

At this point it is worth to compare the equilibrium rates obtained from one-loop (Eq.(13)) and two-loop (Eqs.(17,18)) calculations. In Fig.5 this is shown at $T = 300$ MeV and $\alpha_s = 0.3$ for two flavors. We see that the usual bremsstrahlung contribution originating from the two-loop calculations is of the same order in magnitude as those evaluated at the one-loop level. The contribution from annihilation with scattering process dominates over the entire energy range, and particularly with the increase of the photon energy it is more than an order of magnitude higher than the one-loop contributions. It has to be noted

that there might be further contributions to the hard photon production rate at the same order, coming from three-loop diagrams [19]. Unfortunately these contributions have not been calculated so far due to the complexity of this calculation at finite temperature.

Now it would be very interesting to see how much of the two-loop dominance survives when one convolutes these rates with the space-time history of the chemically equilibrating plasma. For this purpose we first have to determine the two-loop rates for a chemically equilibrating plasma. Considering the possible spin, color and flavor ($N_f = 2$) factors of the scattering diagrams corresponding to the bremsstrahlung and the annihilation with scattering process, where we restrict ourselves to the t-channel diagrams as the exchanged gluon is soft [19], we find for the two-loop bremsstrahlung process (Fig.2b) in a chemically equilibrating plasma

$$E\,\frac{\mathrm{d}N_\gamma}{\mathrm{d}^4x\,\mathrm{d}^3p}\bigg|^{\mathsf{ceq.}}_{\mathsf{brem.}} = \frac{2N_cC_F}{\pi^5}\alpha\alpha_s\left(\frac{4}{7}\lambda_q^2+\frac{3}{7}\lambda_g\lambda_q\right)\left(\sum_f e_f^2\right)T^2e^{-E/T}(J_T-J_L)\ln(2)\ , \qquad (19)$$

and for the annihilation with scattering process (Fig.2c)

$$E\,\frac{\mathrm{d}N_\gamma}{\mathrm{d}^4x\,\mathrm{d}^3p}\bigg|^{\mathsf{ceq.}}_{\mathsf{aws}} = \frac{2N_cC_F}{3\pi^5}\left(\frac{2}{5}\lambda_q^3+\frac{3}{5}\lambda_g\lambda_q^2\right)\alpha\alpha_s\left(\sum_f e_f^2\right)ETe^{-E/T}(J_T-J_L)\ \ . \qquad (20)$$

The dependence of $J_{T,L}$ on the fugacities can be neglected, since they are functions of m_q/m_g only and since the square of the effective quark mass m_q^2, Eq.(16), and of the effective gluon mass m_g^2 are proportional to the gluon fugacity, neglecting the much smaller quark fugacity.

It is to be noted that in Eq.(20) the combination of the different parton fugacities appears in cubic power, compared to the other processes both at one and two-loop, due to the fact that this particular process involves three particles in the entrance channel.

Now to evaluate the yield of the thermal spectrum one should convolute these emission rates with the space time history of the system in the local rest (LR) frame of the fluid as

$$\frac{\mathrm{d}N_\gamma}{\mathrm{d}^2p_T\ \mathrm{d}y} = \int \mathrm{d}^4x\left(E\frac{\mathrm{d}N_\gamma}{\mathrm{d}^4x\,\mathrm{d}^3p}\right)_{\mathsf{LR}}\ \ , \qquad (21)$$

where p_T is the transverse momentum of the photon and y is its rapidity. In the local rest frame the energy of the photon is defined as $E = p_T\cosh(y-\eta)$, where η is the fluid rapidity. The evolution of the plasma is taken into account within the well established hydrodynamic model adopting a boost invariant cylindrically symmetric transverse expansion [50] of the system. In the following section we present our results using the nonequilibrium photon production rates for an expanding and chemically equilibrating plasma with different initial conditions and nuclear profile functions described above.

IV. RESULTS

The parton fugacities for an expanding plasma, likely to be formed at RHIC and LHC energies, are displayed in Figs.3 and 4 with the SSPC initial conditions and the wounded-nucleon profile. The evolution of the parton energy density, transverse velocity and fugacities

with other initial conditions and nuclear profile functions have been discussed in great detail in Refs. [29,35]. It is worth pointing out here that in previous calculations [29,35] a little numerical fluctuation in the evolution of the fugacities around the centre of the plasma at later time has now been corrected using improved numerics in the present calculation.

In Fig.6 we present the thermal photon production from the quark phase as a function of its transverse momentum at RHIC energies with SSPC initial conditions and the wounded-nucleon profile function both in the equilibrium and equilibrating scenario, where we assumed the same initial temperatures in both cases given in Table-I. The contribution from different physical processes discussed in the preceding section can easily be identified from the figure itself. As expected from the equilibrium static rates, the photon spectrum from the equilibrated QGP (see upper panel of Fig.6) is dominated by the annihilation with scattering contribution. According to the prediction of the SSPC model the QGP, likely to be created at RHIC energies, will be far away from chemical equilibrium. Hence the realistic scenario is given by the photon yield from a chemically equilibrating plasma, shown in the lower panel of Fig.6. It can be seen that the most dominant contribution comes from the usual bremsstrahlung processes rather than from the aws and one-loop processes, even though the aws static equilibrium rate was higher by more than an order of magnitude (Fig.5). The reason is obvious as the rate for the aws processes for an equilibrating plasma involves the parton fugacities to cubic power (Eq.(20)) whereas the other processes are only quadratic in the fugacities (Eqs.(14,15,19)), and the fugacities at RHIC are small for the entire life time of the plasma. At higher p_T the one-loop contributions even exceed the aws contribution as energetic photons have their origin in the early hot stage of the plasma, where the fugacities are very small. It is also worthwhile to note that the SSPC model predicts a gluon dominated plasma (see Table-I) implying in general larger contributions from processes involving gluons in the entrance channel. The total thermal photon yield at RHIC dominates over the prompt photon contributions [56] for $p_T \leq 4.5$ GeV. However, if only the one-loop contribution is considered [29] the prompt photons overshadow the thermal photon yield already beyond $p_T \geq 3$ GeV. Since the life time of the plasma at RHIC is small, the photon yield is not affected by the flow [29].

The corresponding results for LHC energies are shown in Fig.7. The photon yields from different processes as well as the total yield are much larger than at RHIC as the life time of the plasma, likely to be created at LHC energy, is expected to be much larger and the the initial temperature, energy density, and fugacities are higher (see Table-I). The upper panel shows the equilibrated scenario, whereas the lower panel applies to the equilibrating one. Now the usual bremsstrahlung and the aws contribution originating from two-loop calculations are very similar in the non-equilibrium case, whereas the one-loop contribution is small at all p_T. The reduced suppression of the contribution due to the aws process compared to RHIC can be understood in the following way. The rate depends linearly on the temperature and cubicly on the fugacities. In addition the aws is also proportional to the energy of the photon. Now with the passage of time the system expands, the temperature falls and the chemical reactions pushes the system towards equilibrium causing the fugacities to increase, though at later time they decrease significantly caused by transverse expansion. Hence, there is a competition between the space-time evolution of the temperature and the fugacities though they are not exactly counterbalanced. Rather, the interplay of these two quantities along with the photon energy dependence causes a reduced suppression of the aws

contribution compared to RHIC.

The prompt photon productions [56] due to lowest order QCD (Born) and inclusive photons (background photons fragmented off high-p_T quark jets) will remain buried under the thermal photon yield for all p_T-values considered here.

Now we would also like to point out here the effect of the transverse flow on the photon production. Due to the transverse flow, the high-p_T photons will not be affected as they have their origin in the early hot stages where the transverse flow is minimal. However, the production of low-p_T photons will be reduced substantially compared to the scenario where there is no transverse flow [29] due to the reduction of the life time of the plasma and the decrease of the fugacities at later times [29,35,36]. However, the reduction of the high-p_T photons due to the small fugacities at early times overwhelms this effect.

In Fig.8 we display the photon yields at RHIC energies with SSPC initial conditions and a Fermi-like profile function both for an equilibrated (upper panel) and an equilibrating (lower panel) plasma. For an equilibrated plasma the photon yield at high-p_T is strongly enhanced compared to that with the wounded profile function, whereas the low-p_T production is similar in both cases. The wounded-nucleon profile function in eq.(12) implies a faster onset of the transverse expansion than the Fermi-like profile function in eq.(11). Hence, using a Fermi-like profile associated with a slower cooling implying a higher temperature, yields an enhanced photon production at high-p_T for an equilibrated plasma. In the case of the equilibrating plasma (lower panel) the high-p_T yields are much less enhanced compared to the wounded profile case. As already discussed, the initial fugacities tabulated in Table-I are not modified for the Fermi-like profile, whereas they are larger for the wounded-nucleon profile. Therefore the equilibrating photon yields at high-p_T are reduced for the Fermi-like profile due to the small values of the parton fugacities as the high-p_T photons have their origin from the initial hot stages. The thermal photons dominate over the prompt photon production as before.

In Fig.9 we display the photon production at LHC energy with SSPC initial conditions and a Fermi-like profile of the system. The slower onset of the transverse expansion allows the system to live a little longer ($\sim$ 12.5 fm/c) [29,35] than for the wounded profile ($\sim$ 10 fm/c) [36]. This results in a larger space-time volume occupied by the plasma in the quark phase than in the wounded-profile case in contrast to RHIC (Fig.8), where the life time is of the same order for both profiles. Since the life time of the plasma is longer, the photon yields for the Fermi-like profile in a fully equilibrated plasma is higher for all momenta (upper panel). The suppression of the photon yields at high-p_T for a chemically equilibrating plasma (lower panel) compared to equilibrium has the same explanation as at RHIC energies. The other aspects like flow and prompt photon production are same as in Fig.7.

In the following we present our results with HIJING initial conditions (see Table-I) along with the Fermi-like profile. If we use the original prediction, *i.e.*, HIJING-I, then the life time of the QGP phase is very small (less than 2 fm/c) for RHIC and 7.5 fm/c for LHC [29]. Also the matter will be very dilute due to the very small initial values of the fugacities at RHIC. Furthermore, for LHC only the fluid beyond 4 fm from the centre participates in flow. Now for HIJING-II initial condition, the life time of the plasma increases substantially both for RHIC ($\sim$ 4 fm/c) and LHC ($\sim$ 12 fm/c). Also the initial fugacities differ by one order of magnitude for RHIC, and are reasonably higher for LHC. For LHC the entire fluid

will participate in the transverse flow since the life time is large and initially the system will approach towards equilibrium but then be driven away from it as soon as the large velocity gradient develops. Fig.10 exhibits the photon production from the equilibrating plasma with HIJING-I initial conditions and a Fermi-like nuclear profile both at RHIC (upper panel) and LHC (lower panel) energies. Because of the very low initial values, the contribution of the different processes are suppressed in both cases. The huge suppression of the aws contribution, depending cubicly on the fugacities, compared to the other processes at RHIC is due to the fact that the fugacities are very small. Also at LHC the strong suppression at high-p_T is due to the low initial values as high-p_T photons are mostly emitted from the initial stages.

Finally the results for an equilibrating plasma with HIJING-II initial conditions are given in Fig.11. Since the initial fugacities are an order of magnitude higher for RHIC, the contributions from each process, particularly from the aws, are enhanced substantially compared to HIJING-I (upper panel). Since the initial fugacities are higher compared to SSPC but the initial temperature is smaller, there is a counterbalance of these two effects, and the total photon production for LHC (lower panel) is almost the same as that using SSPC initial conditions (lower panel of Fig. 9).

V. SUMMARY AND CONCLUSION

We have considered the photon production from a chemically nonequilibrated QGP at RHIC and LHC energies. In particular we have included bremsstrahlung and quark-antiquark annihilation with scattering. The photon production rate due to the latter processes has been calculated recently using the HTL resummation technique by Aurenche et al. [19] in the case of an fully equilibrated QGP. Instead of repeating this calculation in the non-equilibrium plasma, we estimated the non-equilibrium photon production rate simply by assigning fugacity factors, describing the deviation of the parton densities from chemical equilibrium, to the partons in the entrance channels of the matrix elements corresponding to the different processes (annihilation, Compton scattering, bremsstrahlung, annihilation with scattering). Regarding the uncertainties, such as the initial conditions and the shape of the fireball profile in the computation of the photon spectrum, this simplification is justified.

The photon spectra have been calculated from these rates by using a hydrodynamical calculation, describing the space-time evolution of the QGP phase of the fireball, where we have taken into account the transverse expansion of the fireball. The initial conditions for the temperature and the fugacities have been taken from microscopic models (SSPC, HIJING).

We found that the photon yield is reduced by one to three orders of magnitudes compared to the fully equilibrated plasma, assuming the same initial temperature, where the suppression is more pronounced for energetic photons coming from the highly dilute early stage. Whereas the contribution from the annihilation with scattering process dominates the photon production over the entire momentum range in equilibrium, in a chemically non-equilibrated plasma it is suppressed at RHIC energies compared to the bremsstrahlung contribution, which is now dominating, and even to the one-loop (annihilation, Compton scattering) contributions, which is the smallest in equilibrium. The reason for this behavior is that the annihilation with scattering process depends cubicly on the fugacities, which are

very small at RHIC, whereas the other processes only quadratically. At LHC energies, on the other hand, where the fugacities are significantly larger, the annihilation with scattering and the bremsstrahlung contributions are of the same order and exceed the one-loop contributions clearly. Only using the original initial conditions (I) from HIJING, where the fugacities are very small even for LHC, the annihilation with scattering contribution is suppressed compared to the others also at LHC.

We have also investigated the dependence of our results on different initial conditions and the choice of the profile of the fireball. The photon yield can vary by more than an order of magnitude, depending on the choice of the initial conditions, while the dependence on the profile function is weak in the non-equilibrium case.

REFERENCES

[1] B. Müller, The Physics of the Quark-Gluon Plasma, Lecture Notes in Physics **225** (Springer, Berlin, 1985); J. W. Harris and B. Müller, Annu. Rev. Nucl. Part. Sci. **46**, 71 (1996).

[2] R. C. Hwa (Ed.), Quark-Gluon Plasma 1 and 2 (World Scientific, Singapore, 1990 and 1995).

[3] C. Y. Wong, Introduction to High Energy Heavy Ion Collisions (World Scientific, Singapore, 1994).

[4] F. Karsch, Proc. Lattice'99, ⟨hep-lat/9909006⟩, Nucl. Phys. B (in print).

[5] P. Braun-Munzinger, ⟨nucl-ex/9908007⟩; ⟨nucl-ex/9909014⟩.

[6] B. Müller, Nucl. Phys. **A630**, 461c (1998).

[7] G. Domokos, Phys. Rev. D **28**, 123 (1983)

[8] E. V. Shuryak, Phys. Lett. B **78**, 150 (1978).

[9] L. D. McLerran and T. Toimela, Phys. Rev. D **31**, 545 (1985).

[10] K. Kajantie, J. Kapusta, L. D. McLerran, and A. Mekjian, Phys. Rev. D **34** 2746 (1986).

[11] J. Cleymans, J. Fingberg, and K. Redlich, Phys. Rev. D **35** 2153 (1987).

[12] E. Braaten, R. D. Pisarski, and T. C. Yuan, Phys. Rev. Lett. **64**, 2242 (1990).

[13] M. H. Thoma and C. T. Traxler, Phys. Rev. D **56**, 198 (1997); T. Altherr, and P. V. Ruuskanen, Nucl. Phys. **B380**, 377 (1992).

[14] W. Cassing and E. L. Bratkovskaya, Phys. Rep. **308**, 65 (1999).

[15] J. I. Kapusta, P. Lichard, and D. Seibert, Phys. Rev. D **44**, 2774 (1991).

[16] R. Baier, H. Nakkagawa, A. Niegawa, and K. Redlich, Z. Phys. C **53**, 433 (1992); R. Baier, S. Peigne, and D. Schiff, Z. Phys. C **62**, 337 (1994).

[17] P. Aurenche, F. Gelis, R. Kobes, and E. Petitgirard, ⟨hep-ph/9403320⟩.

[18] P. Aurenche, F. Gelis, R. Kobes, and E. Petitgirard, Z. Phys. C **75**, 315 (1996).

[19] P. Aurenche, F. Gelis, R. Kobes, and H. Zaraket, Phys. Rev. D **58**, 085003 (1998).

[20] R. Baier, M. Dirks, K. Redlich and D. Schiff, Phys. Rev. D **56**, 2548 (1997); F. Flechsig, and A. K. Rebhan, Nucl. Phys. B **464**, 279 (1996).

[21] D. K. Srivastava and B. Sinha, Phys. Rev. Lett. **73**, 2421 (1996).

[22] D. K. Srivastava and K. Geiger, Phys. Rev. C **58**, 1734 (1998).

[23] D. K. Srivastava, Eur. Phys. J. C **10**, 487 (1999); D.K Srivastava and B. Sinha, Eur. J. Phys. C **12**, 109 (2000).

[24] F. D. Steffen, ⟨nucl-th/9909035⟩.

[25] D. Yu. Perssounko and Yu. E. Pokrovsky, ⟨hep-ph/9906325⟩.

[26] J. Alam, S. Raha and B. Sinha, Phys. Rep. **273**, 243 (1996); S. Chakrabarty, J. Alam, D. K. Srivastava, B. Sinha, and S. Raha, Phys. Rev. D **46**, 3802 (1992); J. Alam, D. K. Srivastava, B. Sinha, and D. N. Basu, Phys. Rev. D **48**, 1117 (1993); S. Sarkar et. al., Nucl. Phys. A **634**, 206 (1998); J. Alam, S. Sarkar, P. Roy, T. Hatsuda, and B. Sinha, ⟨hep-ph/9909267⟩.

[27] C. T. Traxler and M. H. Thoma, Phy. Rev. C **53**, 1348 (1996).

[28] M. Strickland, Phys. Lett. B **331**, 245 (1994).

[29] D. K. Srivastava, M. G. Mustafa, and B. Müller, Phys. Rev. C **56**, 1064 (1997).

[30] M. G. Mustafa, A. Schäfer, and M. H. Thoma, Phys. Rev. C **61**, 024902 (2000).

[31] For a recent review, see Proceeding of Quark Matter'99, Nucl. Phys. A (in print).

[32] M. H. Thoma, Phys. Rev. D **51**, 862 (1995).

[33] T. S. Biró, E. van Doorn, B. Müller, M. H. Thoma, and X.-N. Wang, Phys. Rev. C **48**, 1275 (1993).
[34] L. Xiong and E. Shuryak, Phys. Rev. C **49**, 2203 (1994).
[35] D. K. Srivastava, M. G. Mustafa, and B. Müller, Phys. Lett. B **396**, 45 (1997).
[36] B. Müller, M. G. Mustafa and D. K. Srivastava, Heavy Ion Physics **5**, 387 (1997).
[37] D. M. Elliot and D. H. Rischke, ⟨nucl-th/9908004⟩.
[38] E. Braaten and R. D. Pisarski, Nucl. Phys. **B337**, 569 (1990), Nucl. Phys. **B339**, 310 (1990); J. Frenkel and J. C. Taylor, Nucl. Phys. **B334**, 199 (1990); J. Frenkel and J. C. Taylor, Nucl. Phys. **B374**, 156 (1992).
[39] H. A. Weldon, Phys. Rev. D **28**, 2007 (1983); C. Gale and J. I. Kapusta, Nucl. Phys. **B357**, 65 (1991).
[40] V. V. Goloviznin and K. Redlich, Phys. Lett. B **319**, 520 (1993).
[41] P. K. Roy, D. Pal, S. Sarkar, D. K. Srivastava and B. Sinha, Phys. Rev. C **53**, 2364 (1996); D. Pal, P. K. Roy, S. Sarkar, D. K. Srivastava and B. Sinha, Phys. Rev. C **55**, 1467 (1999).
[42] D. Pal and M. G. Mustafa, Phys. Rev. C **60**, 034905 (1999).
[43] R. Rückl, Phys. Lett. B **64**, 39 (1976).
[44] P. Lichard, Phys. Rev. D **51**, 6017 (1995).
[45] P. Aurenche, F. Gelis, R. Kobes, and H. Zaraket, Phys. Rev. D **60**, 076002 (1999).
[46] R. Albrecht et al., WA80 Collaboration, Phys. Rev. Lett. **76**, 3506 (1996).
[47] K. J. Eskola, B. Müller, and X. N. Wang, Phys. Lett. B **374**, 20 (1996)
[48] K. J. Eskola and X.-N. Wang, Phys. Rev. **D49**, 1284 (1994).
[49] 1.45 GeV/fm^3 corresponds to the energy density of a fully equilibrated QGP at $T \approx$ 160 MeV.
[50] H. von Gersdorff, L. McLerran, M. Kataja, and P. V. Ruuskanen, Phys. Rev. D **34**, 794 (1986).
[51] X.-N. Wang and M. Gyulassy, Phys. Rev. D **44**, 3501 (1991).
[52] Only in the case of a purely longitudinal expansion the relation $\tau = N\tau_i$ holds [29]. As soon as the transverse expansion sets in, the life time of the plasma is reduced considerably.
[53] R. L. Kobes and G. W. Semenoff, Nucl. Phys. **B260**, 714 (1985); Nucl. Phys. **B270**, 329 (1986).
[54] Here we assumed only up and down quarks to contribute to the photon production, *i.e.*, $\sum_f e_f^2 = 5/9$.
[55] M.E. Carrington, H. Defu, and M.H. Thoma, Eur. Phys. J. C **7** (1999) 347.
[56] J. Cleymans, E. Quack, K. Redlich, and D. K. Srivastava, Int. J. Mod. Phys. A **10**, 2941 (1995).

TABLES

TABLE I. Initial conditions for the hydrodynamical expansion phase in central collision of two gold nuclei at BNL RHIC and CERN LHC energies from SSPC and HIJING models.

Energy	τ_i (fm/c)	T_i (GeV)	$\lambda_g^{(i)}$ -	$\lambda_q^{(i)}$ -	ϵ_i (GeV/fm^3)
SSPC					
RHIC	0.25	0.668	0.34	0.064	61.4
LHC	0.25	1.02	0.43	0.082	425
HIJING					
RHIC, I	0.7	0.55	0.05	0.008	4.0
RHIC, II	0.7	0.40	0.53	0.083	11.7
LHC, I	0.5	0.82	0.124	0.02	48.6
LHC, II	0.5	0.72	0.761	0.118	176

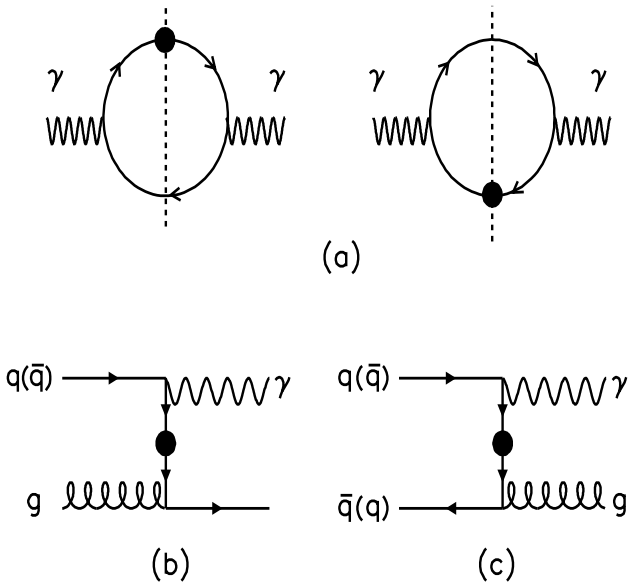

FIG. 1. **(a)** One-loop photon self-energy diagrams with a HTL resummed quark propagator. Cutting these one-loop diagrams along the dashed lines leads to **(b)** Compton scattering and **(c)** annihilation processes for the photon production.

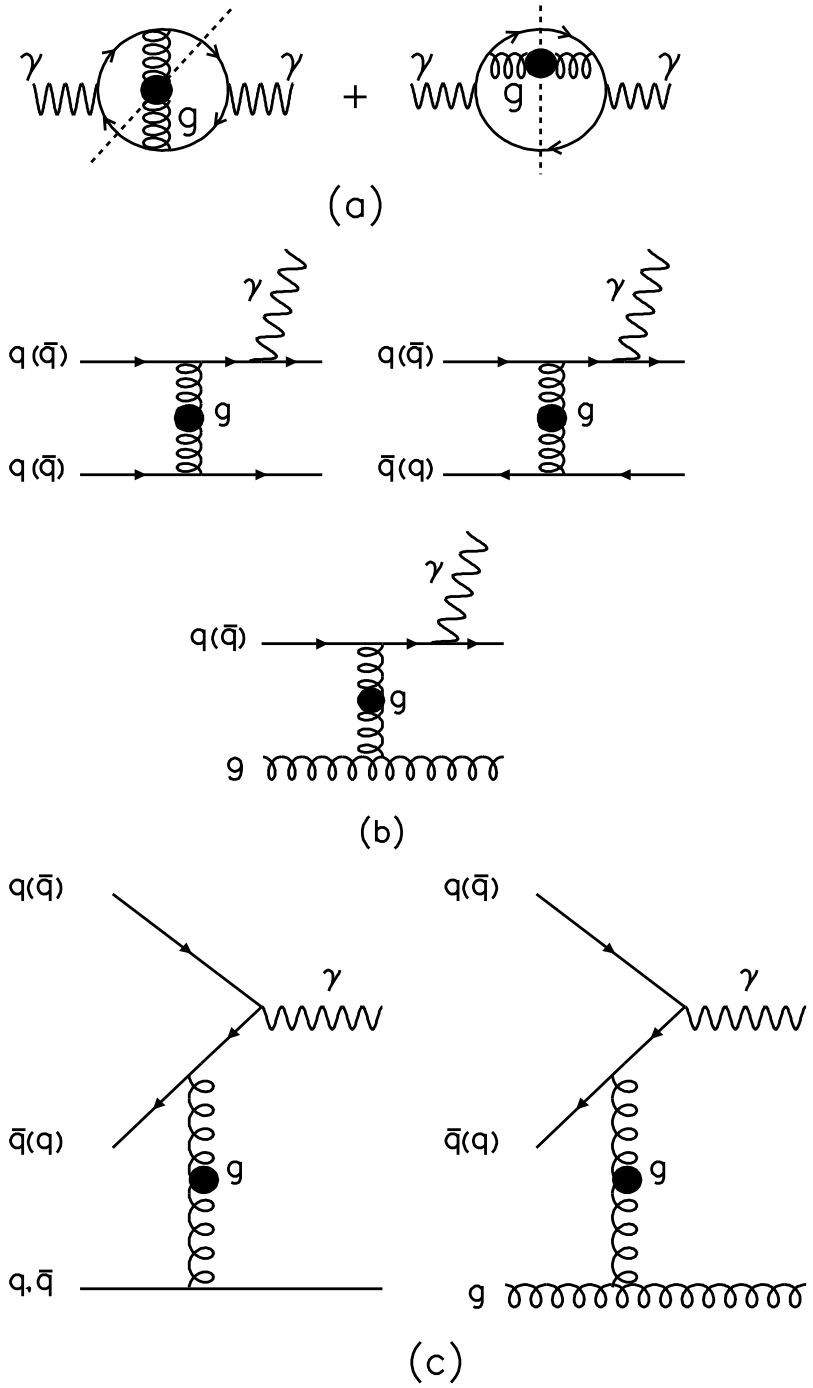

FIG. 2. **(a)** Simplified two-loop photon self-energy diagrams with bare vertices and propagators everywhere except for the gluon propagator since the gluon can be soft. Cutting these two-loop diagrams along the dashed lines leads to **(b)** bremsstrahlung and **(c)** annihilation with scattering off a quark, antiquark or gluon.

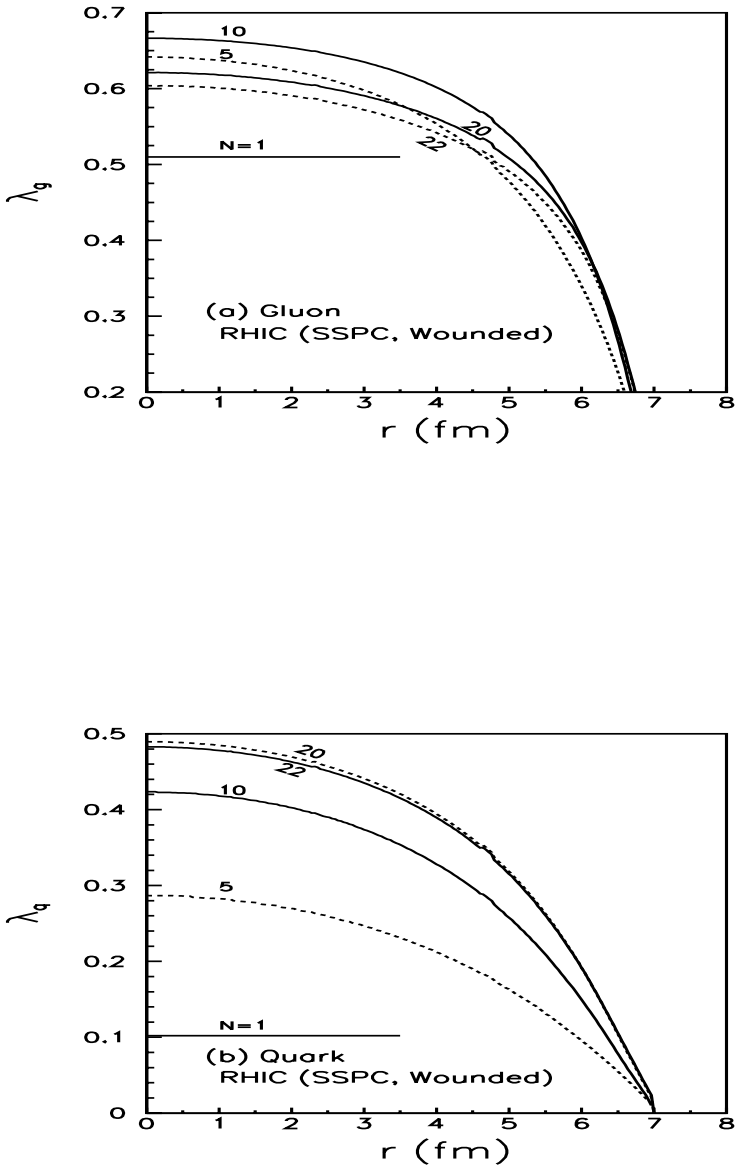

FIG. 3. Evolution of **(a)** gluon and **(b)** quark fugacities along constant energy density contours for a transversely expanding plasma at RHIC energies. N denotes the time [29], and the energy density contours are the solutions of the hydrodynamic equations with the wounded-nucleon profile function and the initial conditions obtained from the SSPC model.

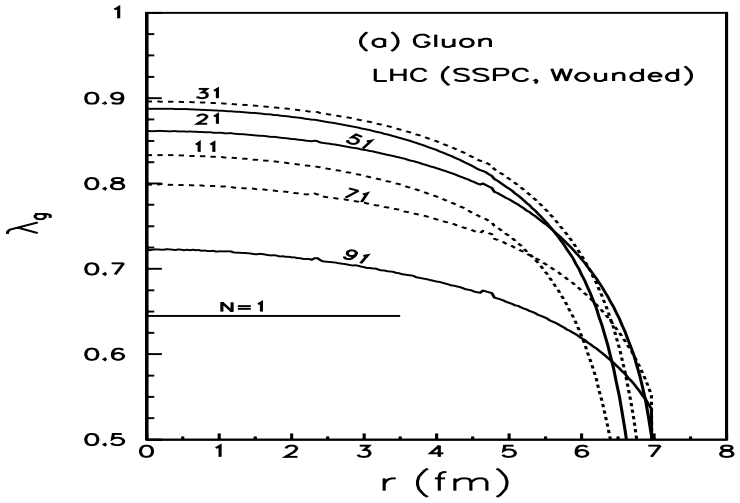

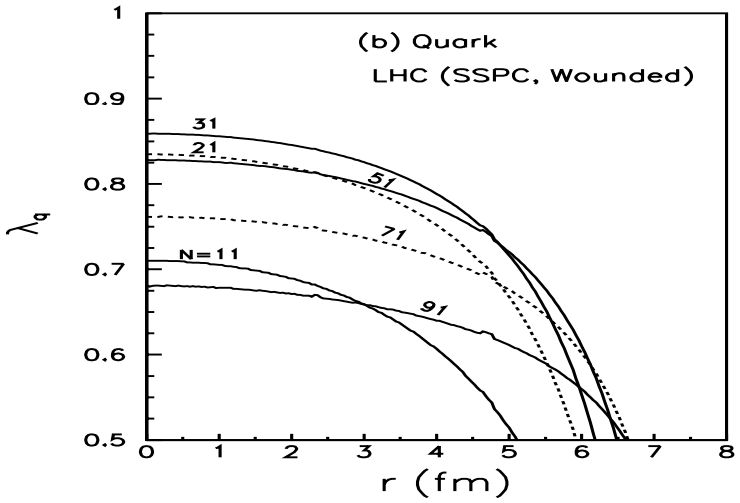

FIG. 4. Same as Fig.3 for LHC energies.

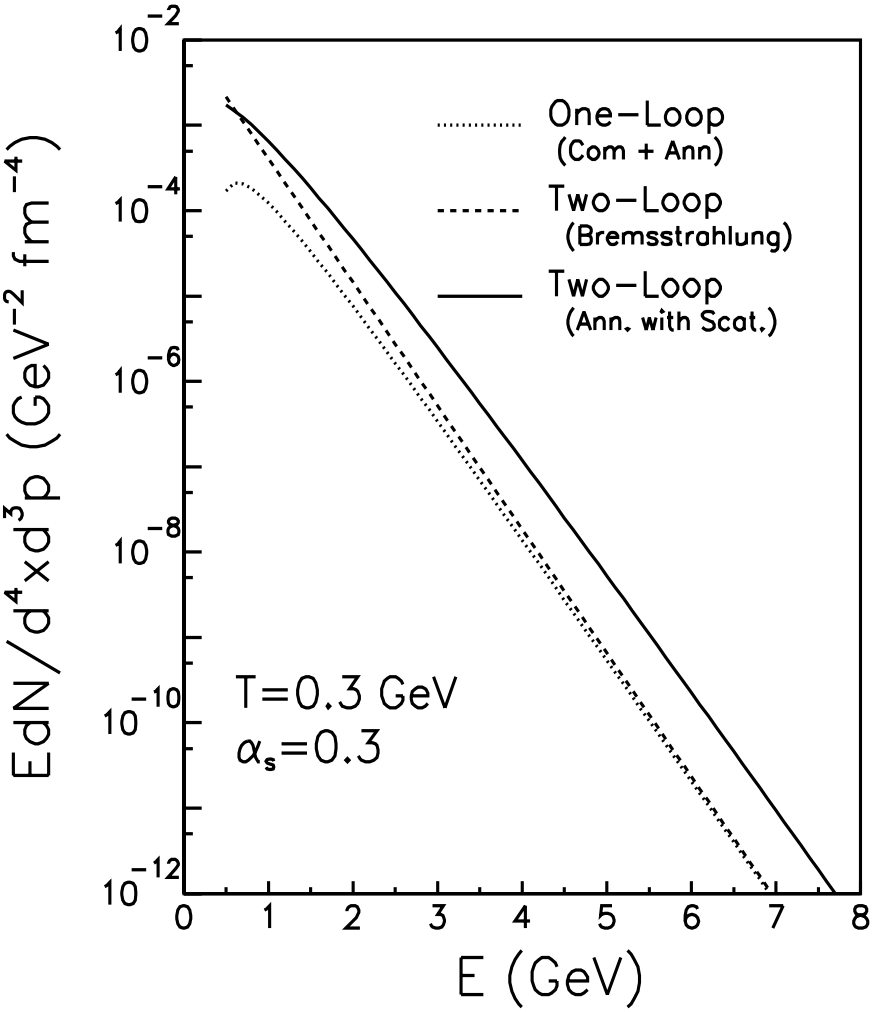

FIG. 5. Equilibrium photon production rate from various processes in the QGP originating from one- and-two loop self-energy diagrams at $T = 300$ MeV and $\alpha_s = 0.3$.

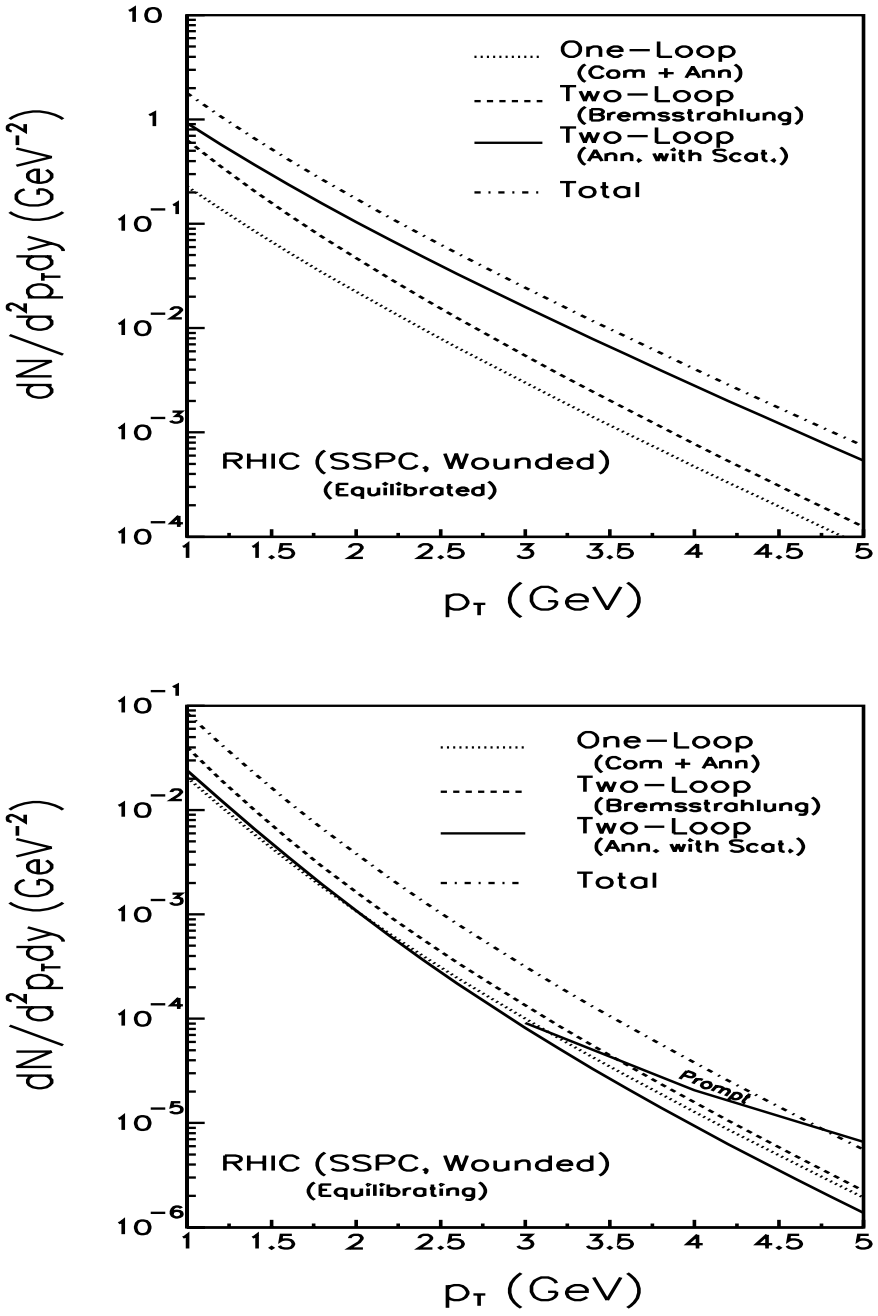

FIG. 6. Photon spectra from various processes at RHIC energies with SSPC initial conditions and the wounded-nucleon profile function. The upper panel corresponds to complete equilibrium, whereas the lower panel represents the chemically equilibrating scenario. In the lower panel the prompt photon production has also been included.

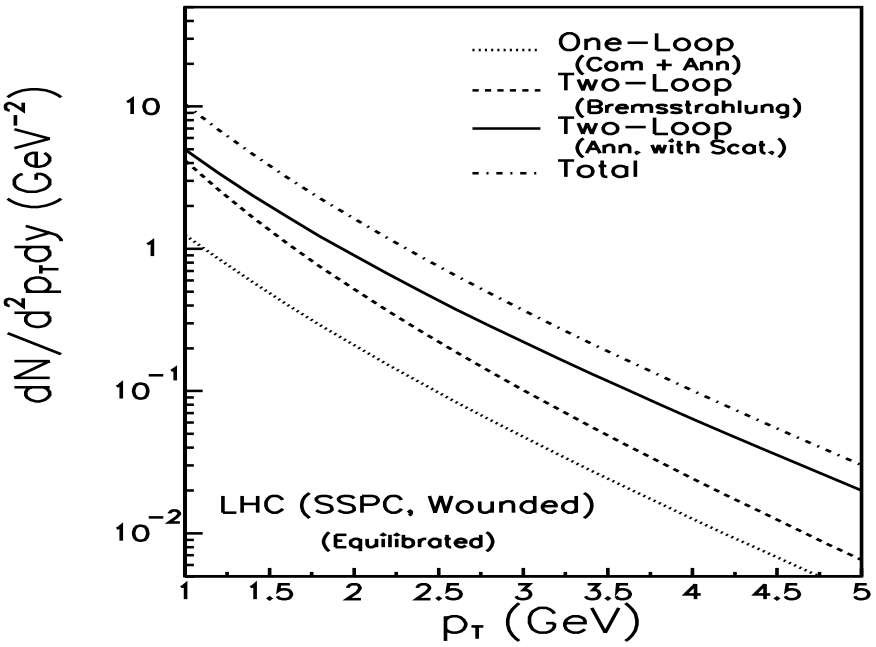

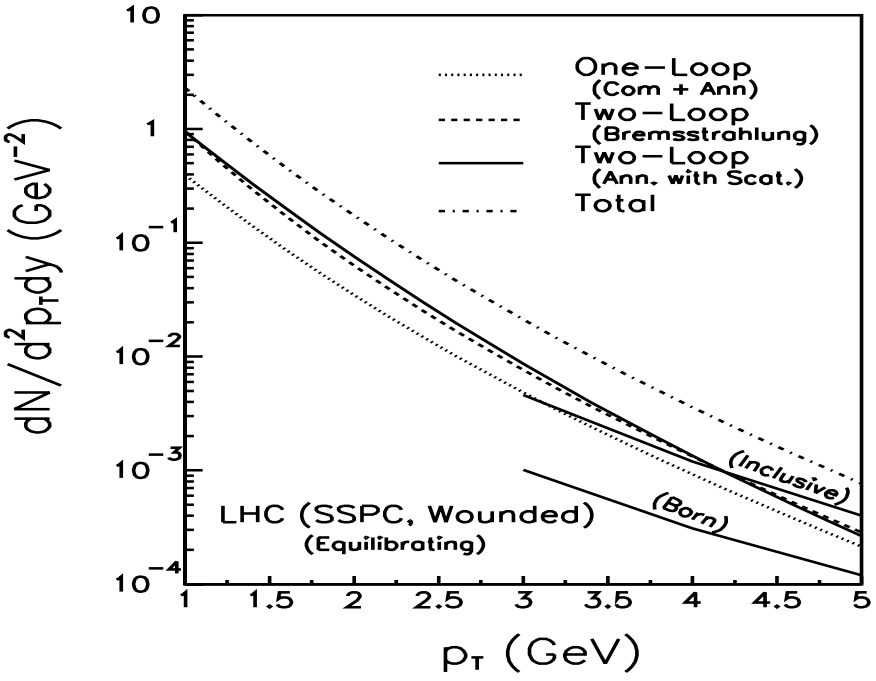

FIG. 7. Same as Fig.6 for LHC energies.

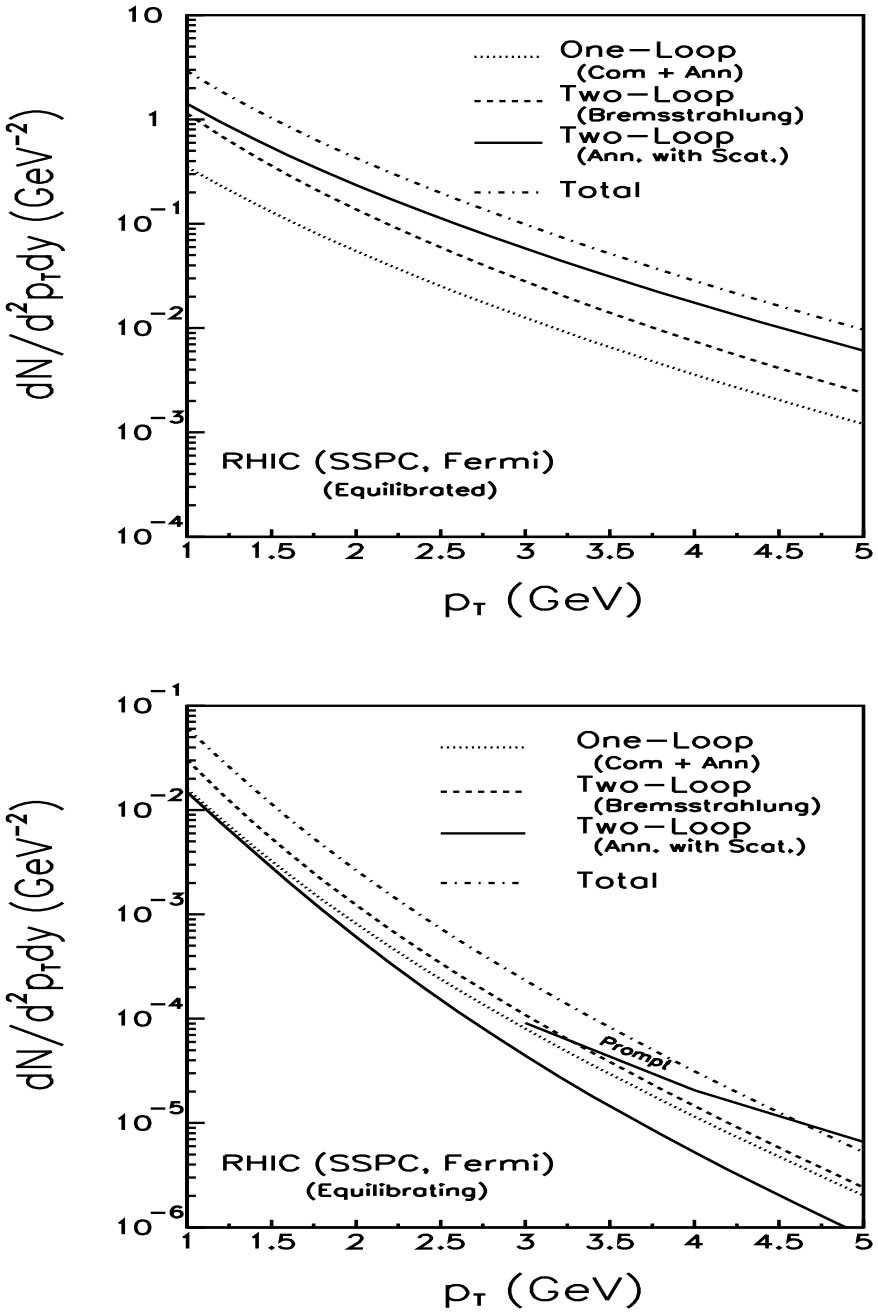

FIG. 8. Photon spectra from various processes at RHIC energies with SSPC initial conditions and the Fermi-like profile function. The upper panel represents the fully equilibrated scenario, whereas the lower panel corresponds to the chemically equilibrating scenario.

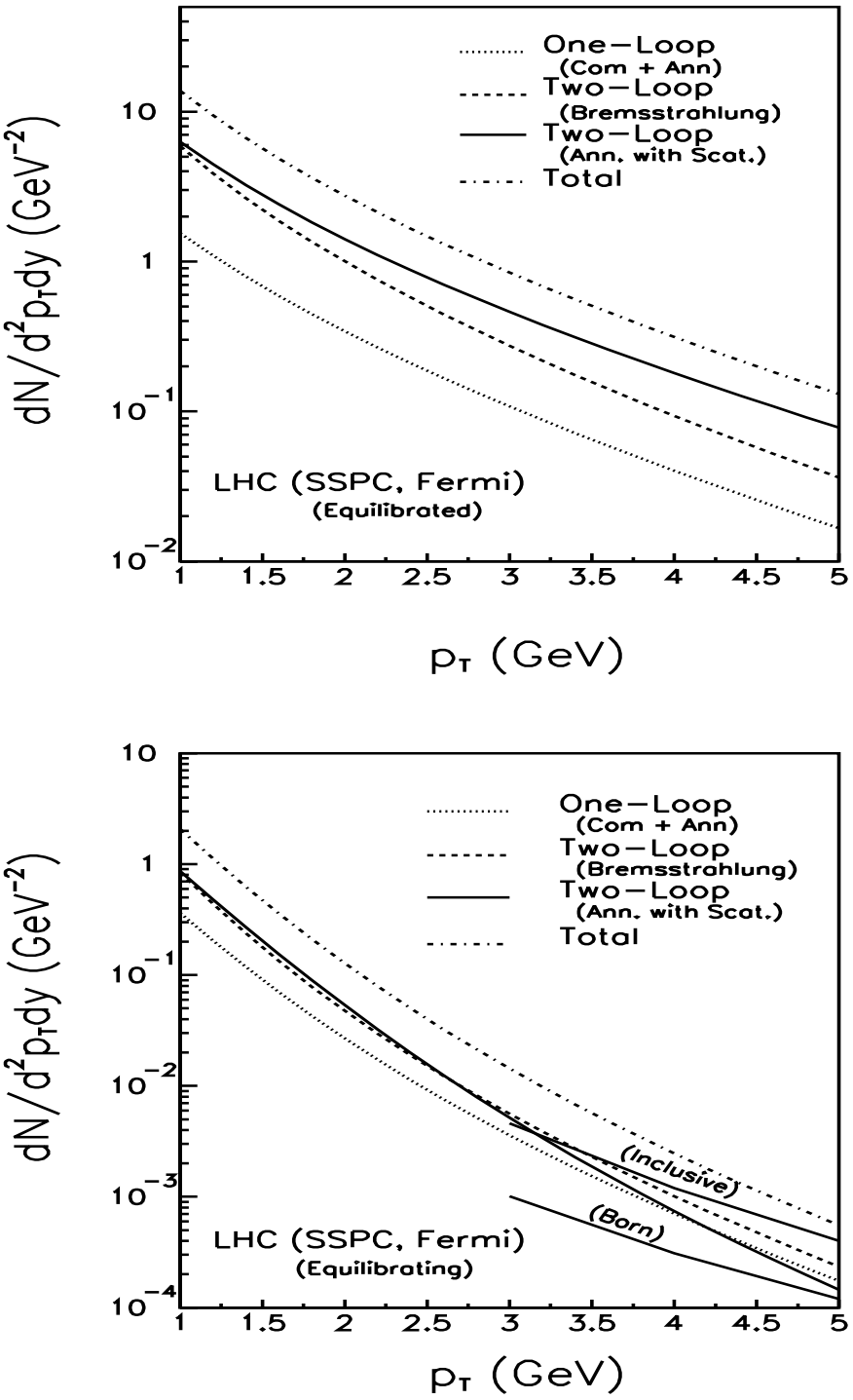

FIG. 9. Same as Fig.8 for LHC energies.

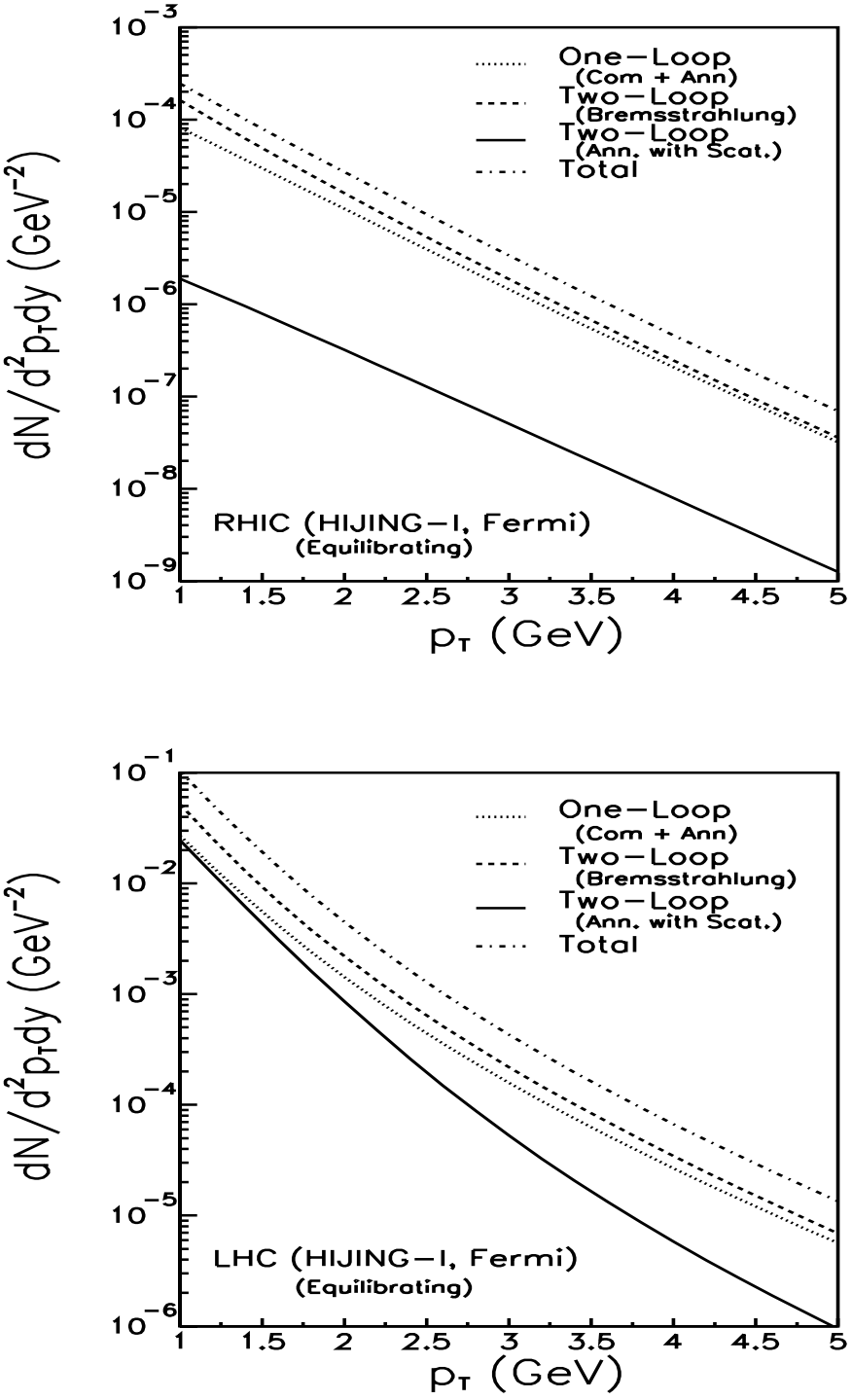

FIG. 10. Photon spectra for a chemically equilibrating plasma at RHIC (upper panel) and LHC (lower panel) energies with HIJING-I initial conditions and Fermi-like profile function.

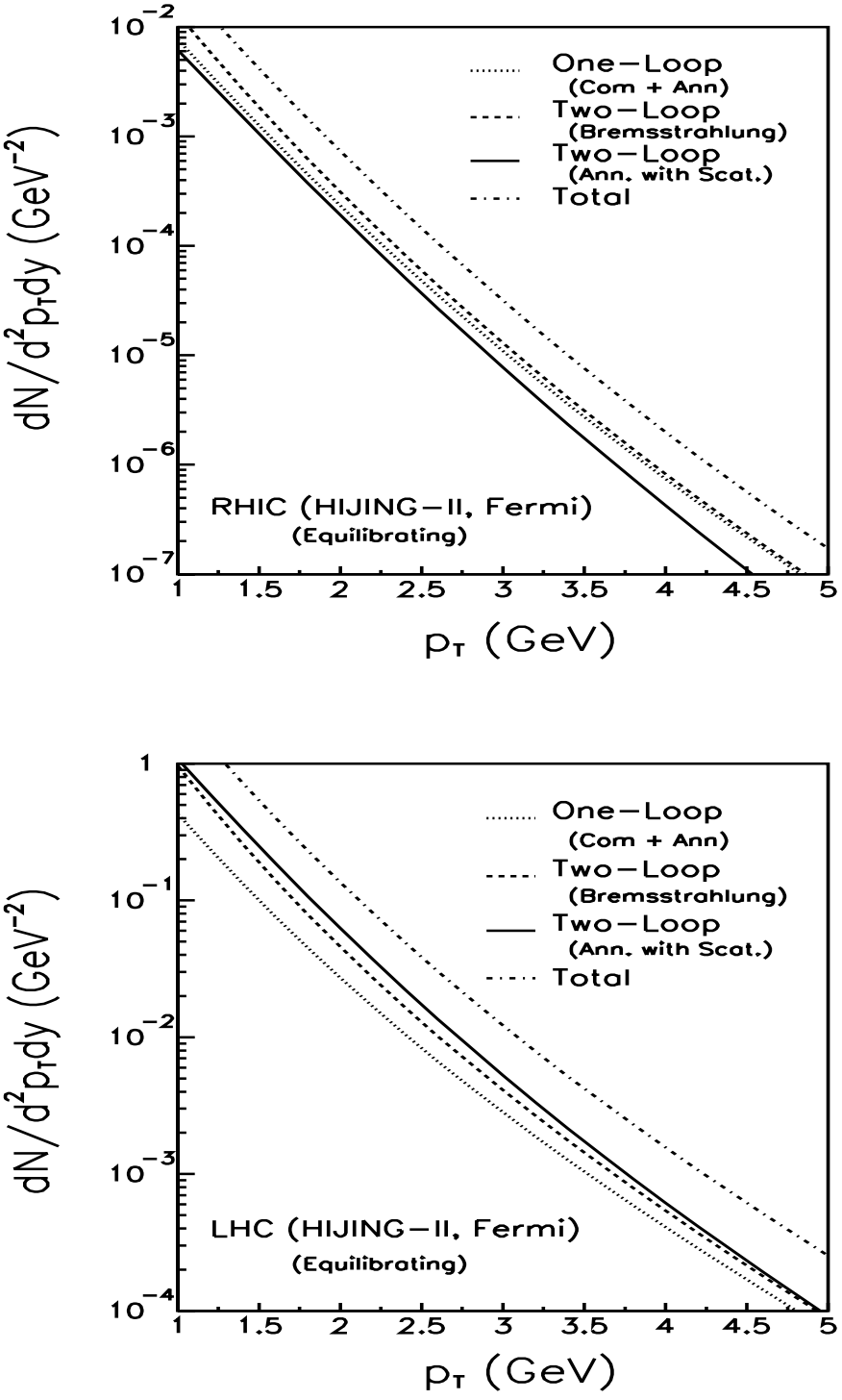

FIG. 11. Same as Fig.10 with HIJING-II initial conditions.